In-Plane and Interfacial Thermal Conduction of Two-Dimensional Transition-Metal Dichalcogenides

Yifei Yu,[1,†] Tamzid Minhaj,[1,†] Lujun Huang,[1] Yiling Yu,[1] and Linyou Cao[1,2,3,*]

[1] *Department of Materials Science and Engineering, North Carolina State University, Raleigh, North Carolina 27695, USA*

[2] *Department of Physics, North Carolina State University, Raleigh, North Carolina 27695, USA*

[3] *Department of Electrical and Computer Engineering, North Carolina State University, Raleigh, North Carolina 27695, USA*

(Received 23 September 2019; revised manuscript received 10 January 2020; accepted 18 February 2020; published 24 March 2020)

We elucidate the dependence of the in-plane and interfacial thermal conduction of two-dimensional (2D) transition-metal dichalcogenide (TMDC) materials (including MoS_2, WS_2, and WSe_2) on the materials' physical features, such as size, layer number, composition, and substrates. The in-plane thermal conductivity k is measured at suspended 2D TMDC materials and the interfacial thermal conductance g is measured at materials supported on substrates, both through Raman thermometry techniques. The thermal conductivity k increases with the radius R of the suspended area following a logarithmic scaling as $k \sim \log(R)$. k also shows a substantial decrease from monolayer to bilayer, but only changes slightly with a further increase in the layer number. In contrast, the interfacial thermal conductance g has a negligible dependence on the layer number, but g increases with the strength of the interaction between 2D TMDC materials and the substrate, substantially varying among different substrates. The result is consistent with theoretical predictions and clarifies much inconsistence in the literature. This work provides useful guidance for thermal management in 2D TMDC materials and devices.

DOI: 10.1103/PhysRevApplied.13.034059

I. INTRODUCTION

Two-dimensional (2D) transition-metal dichalcogenide (TMDC) materials, such as MoS_2, WS_2, $MoSe_2$, and WSe_2, show remarkable electrical [1] and optical properties [2], and bear great promise for the development of devices in a wide range of fields, including integrated circuitry [3], optoelectronics [4], spintronics [5], piezoelectricity [6], and thermoelectricity [7]. One important issue for device development is to manage the thermal dissipation in 2D TMDC materials, which is expected to be a major bottleneck for the device performance due to the atomically thin dimension of the materials. However, a fundamental understanding of the thermal conduction in 2D TMDC materials has remained relatively limited [8], which has limited the development of strategies for effective thermal management. For instance, whereas there are numerous studies on the in-plane thermal conductivity of 2D TMDC materials, the results show substantial inconsistencies. The in-plane thermal conductivity of MoS_2 reported in the literature varies by one order of magnitude in the range of 13–120 W/m K [9–12], and there is no clear indication of the cause of the inconsistence, other than speculating on differences in the quality of the materials studied or in the measurement techniques. Additionally, the correlation between the thermal conduction and physical features of 2D TMDC materials, such as size, composition, and layer number, is elusive. Knowledge of the correlation would provide useful guidance for thermal management in 2D TMDC materials and devices.

Here, we elucidate the dependence of the in-plane thermal conductivity and interfacial thermal conductance of 2D TMDC materials on the materials' physical features with Raman thermometry. We demonstrate that the in-plane thermal conductivity k increases with the size R of the materials, following a logarithmic scaling, as $k \sim \log(R)$, and we elucidate the dependence of k on the layer number and composition. Additionally, we show that the interfacial thermal conductance g has a negligible dependence on the layer number, but increases with the strength of the interaction between 2D TMDC materials and substrates. Our results are consistent with the prediction of many theoretical studies and clarify many inconsistencies in previous studies.

*linyoucao@gmail.com

†Y. Yu and T. Minhaj contributed equally to this work.

II. EXPERIMENTAL SECTION

A. Synthesis and transfer TMDC flakes

All TMDC flakes are obtained from a 2D layer made through chemical vapor deposition (CVD), as reported in Ref. [13]. The transfer of TMDC flakes follows a surface-energy-assisted transfer approach that we have developed previously [14]. In a typical transfer process, 9 g of polystyrene (PS) with a molecular weight of 280 000 g/mol is dissolved in 100 ml of toluene, and then the PS solution is spin-coated (3000 rpm for 60 s) on the as-grown substrate (SiO_2/Si). This is followed by baking at 80−90 °C for 1 h. A water droplet is then dropped at the edge of the original substrate. Due to different surface energies of the TMDC flakes and the substrate, water molecules can penetrate the interface, resulting in the delamination of the PS-monolayer assembly. We can pick up the polymer/TMDC flakes with tweezers and transfer them to the quartz substrate with prepatterned holes. After that, we bake the transferred PS-monolayer assembly at 130 °C for 15 min. Finally, PS is removed by gently rinsing with toluene several times.

B. Raman characterization

A Horiba Labram HR800 system with excitation wavelengths of 442 or 532 nm are used to measure the Raman spectra of 2D TMDC materials. The temperature-dependent Raman measurements are carried out with the materials placed on Linkam heating stage (THMS600) with controlled temperature, and the incidence used for the measurement is a focused 532 nm laser with a power of no more than 90 mW, at which the laser-induced temperature increase is usually no more than 20 °C. All power-dependent Raman measurements for the suspended samples are performed at room temperature using a focused 442 nm laser with a radius of 0.66 μm, and those for the supported samples using a focused 532 nm laser with a radius of 0.52 μm.

III. RESULTS AND DISCUSSION

We start by studying single-crystalline MoS_2 flakes grown using a CVD process reported previously [13]. We measure the in-plane thermal conductivity and interfacial thermal conductance of the flakes with a well-established Raman thermometry method [15,16]. The interfacial thermal conductance (ITC) is measured at MoS_2 flakes supported on substrates, while the in-plane thermal conductivity is measured at suspended flakes that are prepared by transferring the MoS_2 flakes from growth substrates (either sapphire or Si/SiO_2) onto a quartz substrate prepatterned with micrometer-scale holes [14]. The use of quartz substrates is to minimize interference of the incident light with light reflected back from the bottom of the hole, which would otherwise cause substantial error in the evaluation of the absorption efficiency. Figure 1(a) shows a schematic illustration of the measurement configuration and typical optical images of the substrate-supported and suspended MoS_2 flakes. Raman thermometry involves the measurement of a power shift rate (PSR), i.e., the dependence of the Raman frequency shift on absorbed incident laser power, and a Raman temperature coefficient (TC), i.e., the dependence of the Raman frequency shift on temperature [Fig. 1(b)]. As the atomically thin materials are very vulnerable, we ensure no material degradation during the measurement for every flake studied by confirming the Raman spectra collected before and after the thermometry measurement are similar. The accuracy of Raman thermometry hinges on precise information about the size w of the focused incident laser beam and the absorption efficiency α of the flakes for the incident laser [17]. We determine the value of w by mapping the Raman intensity across the sharp edge of a gold pad deposited on silicon substrates [Fig. 1(c)]. We also calculate the absorption efficiency α using the refractive index of 2D MoS_2 reported previously [18], as shown in Fig. 1(d). We confirm that the optical response of 2D MoS_2 calculated using the refractive index matches the result of experimental measurements reasonably well (Fig. S1 within the Supplemental Material [19,20]). The calculated absorption efficiency is also consistent with that reported in Ref. [21].

We extract the in-plane thermal conductivity k and interfacial thermal conductance g by fitting experimental results to an analytical model derived from the Fourier equation of heat conduction. Briefly, we consider the thermal conduction in the flakes to be diffusive. As a result, the thermal conduction of the suspended flakes under the incidence of a focused Gaussian laser beam is governed by the following differential equations in a cylindrical coordinate [15]:

$$kt\frac{1}{r}\frac{\partial}{\partial r}\left(r\frac{\partial T}{\partial r}\right)+\frac{\alpha Q}{\pi w^2}\exp\left(-\frac{r^2}{w^2}\right)=0 \quad (r\le R), \quad (1)$$

$$kt\frac{1}{r}\frac{\partial}{\partial r}\left(r\frac{\partial T}{\partial r}\right)-g(T-T_0)=0 \quad (r>R), \quad (2)$$

where T_0 is the ambient temperature, Q is the incident power, R is the radius of the suspended area, and t is the thickness of the flakes. We also have the differential equation governing the heat dissipation of the supported flakes under the incidence of a focused Gaussian laser beam:

$$kt\frac{1}{r}\frac{\partial}{\partial r}\left(r\frac{\partial T}{\partial r}\right)-g(T-T_0)+\frac{\alpha Q}{\pi w^2}\exp\left(-\frac{r^2}{w^2}\right)=0. \quad (3)$$

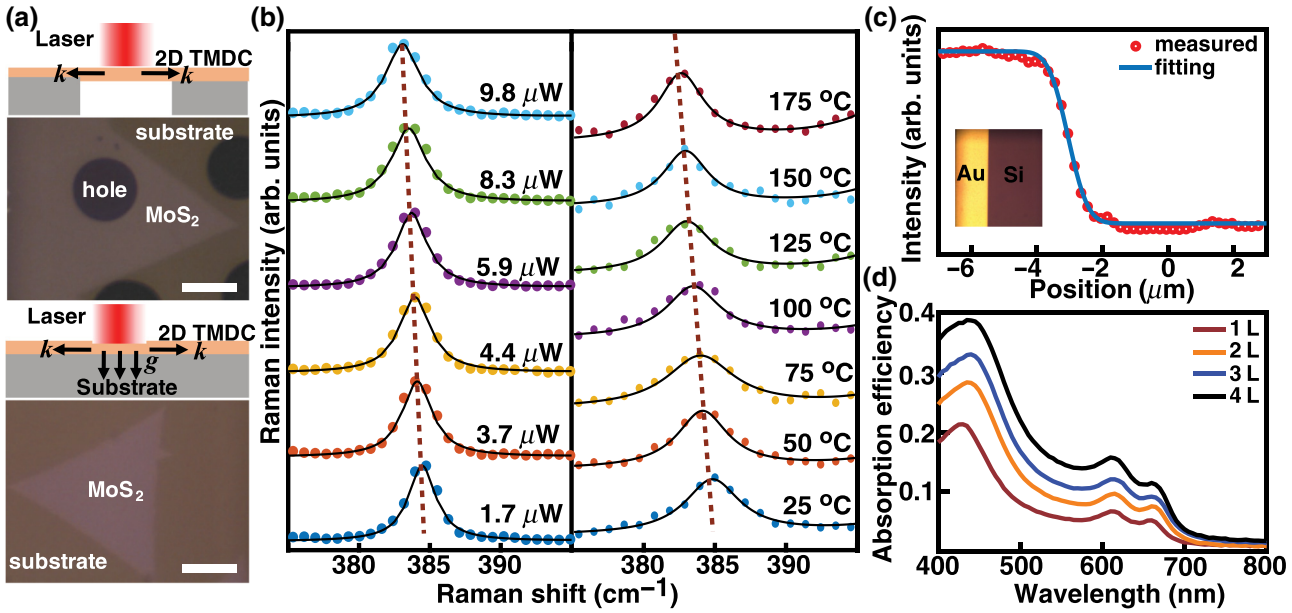

FIG. 1. Raman thermometry measurement for in-plane and interfacial thermal conduction of 2D TMDC materials. (a) Configuration for the Raman thermometry measurement of in-plane thermal conductivity k and interfacial thermal conductance g at suspended (top) and supported (bottom) 2D TMDC materials, and typical optical images for suspended and supported MoS_2 flakes. Scale bar is 10 μm. (b) Dependence of Raman shift of E^1_{2g} peak of suspended monolayer MoS_2 as a function of absorbed laser power (left) and temperature (right). Power-dependent Raman spectra are collected using a focused 442 nm laser with radius of 0.66 μm at room temperature. Temperature-dependent Raman spectra are collected using a 532 nm laser with a power of 90 μW, which is expected to generate temperature increase of no more than 20 °C. Dashed lines serve as a guide to the eye. (c) Measured and fitted spatial distribution of Raman intensity across a sharp edge of a gold pad deposited on Si substrates, which is shown in the inset. (d) Calculated spectral absorption efficiency of suspended MoS_2 flakes with different layer numbers.

By applying appropriate boundary conditions, we can determine the temperature of the suspended flakes to be

$$T(r)=\frac{\alpha Q\{1-\exp[-(r^2/w^2)]\}}{2\pi kR\sqrt{b}t}\frac{K_0\left(\sqrt{b}r\right)}{K_1\left(\sqrt{b}R\right)}+T_0 \quad (r\geq R), \tag{4}$$

$$T(r)=T_1+\frac{\alpha Q}{2\pi kt}\ln\left(\frac{R}{r}\right)+\frac{\alpha Q}{4\pi kt}\left[Ei\left(-\frac{r^2}{w^2}\right)-Ei\left(-\frac{R^2}{w^2}\right)\right] \quad (r\leq R), \tag{5}$$

where $b=g/(kt)$ and T_1 is the temperature at $r=R$ that may be obtained by substituting $r=R$ into Eq. (4). I_0, K_0, and Ei are the zeroth-order modified Bessel function of the first kind, the modified Bessel function of the second kind, and exponential integral functions, respectively. By the same token, we can find the temperature of the supported flakes as

$$T(r)=\frac{\alpha Q}{kt\pi w^2}\int_0^\infty M(k,g,r,y)\exp\left(-\frac{y^2}{w^2}\right)ydy+T_0, \tag{6}$$

$$M(k,g,r,y)=K_0\left(\sqrt{b}r\right)I_0\left(\sqrt{b}y\right) \quad (y\leq r), \tag{7}$$

$$M(k,g,r,y)=I_0\left(\sqrt{b}r\right)K_0\left(\sqrt{b}y\right) \quad (r\leq y). \tag{8}$$

It is worthwhile noting that some previous studies on Raman thermometry use an incorrect equation for the laser-induced temperature distribution of substrate-supported 2D materials due to the application of incorrect boundary conditions [15]. The in-plane thermal conductivity k and the interfacial thermal conductance g can be determined by fitting the Raman measurement result to the model. More specifically, we experimentally find out the temperature of the flakes under the incidence of a focused Gaussian laser using Raman spectroscopy. Then, we can extract the values of k and g by fitting the temperature obtained from Raman measurements with a Gaussian-weighted temperature:

$$T_m=\frac{\int_0^\infty T(r)\exp\left(-\frac{r^2}{w^2}\right)rdr}{\int_0^\infty \exp\left(-\frac{r^2}{w^2}\right)rdr}. \tag{9}$$

This analytical model involves some assumptions and approximations, but we find all of them are reasonable in

our experiment. First, it assumes that the temperature of the substrate does not change during the Raman measurement. For our suspended flakes, the radius of the focused laser beam (for instance, the radius of the focused 442 nm laser is 0.66 μm) is much smaller than the size of the suspended area, and we confirm that the majority of the laser-induced temperature increase is confined in the suspended area, as illustrated in Fig. S2 within the Supplemental Material [20]. In experiments, we obtain similar thermal conductivity at the MoS_2 flakes suspended on the holes in either quartz or gold substrates. This indicates that the thermal conduction in the substrate has a negligible influence on the heat dissipation of the suspended flakes, which confirms a very mild temperature increase at the substrate. For the supported flakes, we monitor the Raman spectra of the substrate during measurements and confirm that the temperature increase at the substrates studied is negligible relative to the temperature increase in the flakes (Fig. S3 within the Supplemental Material [20]). Second, the model ignores heat dissipation through pathways other than thermal conduction, including thermal radiation and thermal convection. In our system, the thermal power dissipated by thermal radiation is estimated to be no more than 0.11 W/cm^2, which is more than four orders of magnitude lower than that of the absorbed incident power. We also find no difference in the laser-induced temperature increase at the suspended flakes under both ambient pressure and vacuum (<0.01 Torr, Fig. S4 within the Supplemental Material [20]). This indicates a negligible contribution of thermal convection, which strongly depends on pressure, to the heat dissipation. Additionally, the model does not consider the variation in the absorption efficiency α with temperature. This is reasonable because the temperature increase in our experiment is not huge (usually <120 °C), and the change in the absorption efficiency is expected to be no more than 10% [22].

We measure the thermal conductivity at the monolayer MoS_2 flakes suspended on holes with different sizes. Figures 2(a) and 2(b) show typical PSR and TC measured at the suspended MoS_2 flakes, and the thermal conductivity derived from the measurement results are plotted in Fig. 2(c). Tabulated measurement results and related thermal conductivities for the suspended MoS_2 flakes are provided in Table S1 within the Supplemental Material [20]. MoS_2 has two major characteristic Raman peaks, E^1_{2g} (~385 cm^{-1}) and A_{1g} (~405 cm^{-1}). We confirm that the measurement for either peak of the suspended flakes usually gives rise to similar thermal conductivities (Fig. S5 within the Supplemental Material [20]). However, the measurement of E^1_{2g} is generally more credible because the A_{1g} peak is susceptible to the effects of doping and can be affected by impurities or adsorbents. Therefore, we focus on the E^1_{2g} peak in this work. Significantly, the thermal conductivity monotonically increases with the suspended size. The size dependence of the thermal conductivity

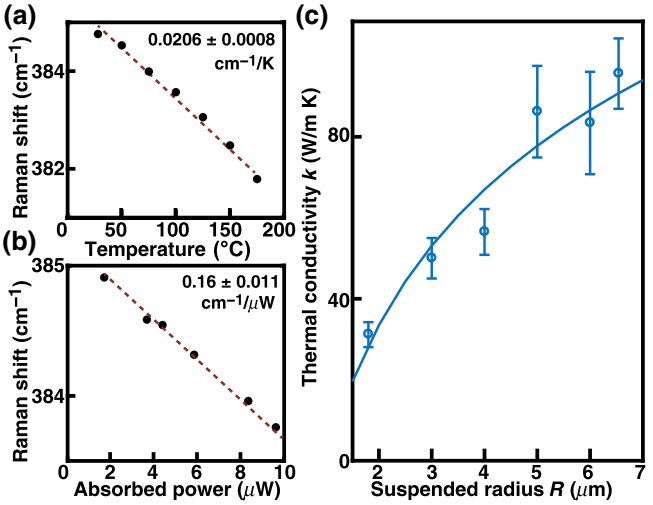

FIG. 2. Size-dependent thermal conductivity of monolayer MoS_2. Typical shift of E^1_{2g} Raman peak as a function of (a) temperature and (b) adsorbed incident laser power. Dots are experimental measurements, and the dashed line is a fit of the experimental results. (c) Thermal conductivity of monolayer MoS_2 as a function of suspended size. Solid line is logarithmic fitting of mean value of measurements.

may be reasonably fitted with a logarithmic scaling as $k \sim \log(R)$. Our result is consistent with theoretical predictions. Numerous theoretical studies predict that the thermal conductivity of two-dimensional Fermi-Pasta-Ulam (FPU) rectangles and disk lattices diverge with size following a logarithmic scaling [23–27]. In particular, recent studies explicitly predicted a logarithmic size scaling in the thermal conductivity of 2D TMDC materials [28,29]. Our result is also consistent with the measurement of suspended graphene ribbons, which show a logarithmic size scaling in thermal conductivity [30,31]. The logarithmic scaling is due to the anharmonicity of phonon potential and boundary scattering in 2D materials. While the phonon mean free path of 2D TMDC materials is reported to be tens of nanometers [32], orders of magnitude smaller than the suspended size in our work, the value represents an average of effective mean free path of a broad spectrum of phonons with different frequencies and polarizations. According to theoretical calculations [32], low-frequency phonons, which have a long mean free path, may play a significant role in the thermal conductivity of 2D materials. More low-frequency thermal phonons may be excited with increasing sample size, leading to an increase in the thermal conductivity.

We also measure the thermal conductivity of suspended MoS_2 flakes with different numbers of layers. The layer number of the flakes is identified by a combination of optical contrast and Raman measurements, as illustrated in the insets of Figs. 3(a) and 3(b). Similar to the measurement for the monolayer, the power-dependent Raman spectra for

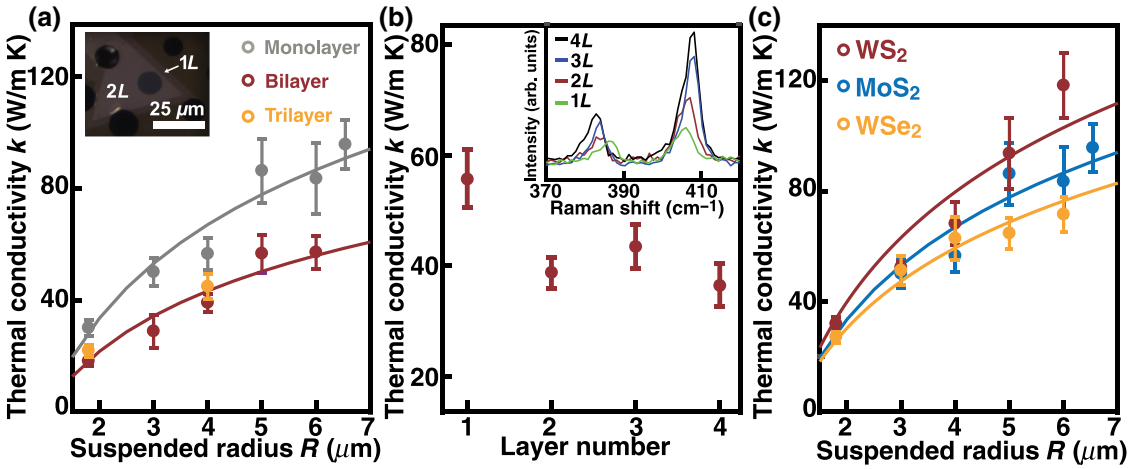

FIG. 3. Layer and composition dependence of thermal conductivity in 2D TMDC materials. (a) Thermal conductivity of bilayer MoS_2 as a function of suspended size (red color). Solid line is logarithmic fitting of $k \sim \log(R)$. Results in gray are size-dependent thermal conductivity of monolayer MoS_2. Also plotted are results collected from trilayer MoS_2 flakes (orange color). Inset: a typical optical image of suspended bilayer MoS_2 flakes, in which the bilayer can be found to show distinct optical contrast from that of monolayers. (b) Thermal conductivity of MoS_2 flakes as a function of layer number. All results collected from flakes suspended on holes with radius of 4 μm. Inset is the Raman spectra collected from these flakes with different layer numbers. (c) Thermal conductivity of monolayer WS_2 (red color) and WSe_2 (orange color) as a function of suspended size. Also plotted is the thermal conductivity of MoS_2 (blue color). Solid lines are associated logarithmic fitting of $k \sim \log(R)$.

multilayered MoS_2 are collected at room temperature using a 442 nm laser with a radius of 0.66 μm at room temperature, and the temperature-dependent Raman spectra are collected using a 532 nm laser with a power expected to generate a temperature increase of no more than 20 °C. We obtain the thermal conductivity by fitting the measurement result with Eq. (9). Figure 3(a) shows the thermal conductivity of bilayer MoS_2 flakes as a function of the suspended size (red dots). Similar to the monolayer counterpart, the bilayer thermal conductivity increases with the suspended size, and the size dependence may be reasonably fitted as $k \sim \log(R)$. While it is difficult to prepare enough suspended trilayers and tetralayers for systematic studies, the result we obtain from a limited number of trilayer and tetralayer samples implies a logarithmic size scaling as well (see Table S1 within the Supplemental Material [20] for the PSR and TC measurement results of few-layer MoS_2). Measurement at flakes with different layer numbers also allows us to elucidate the dependence of the thermal conductivity on the layer number. To illustrate this idea, we compare the thermal conductivity of suspended MoS_2 flakes with different layer numbers, but the same size (4 μm, without losing generality), as shown in Fig. 3(b). The thermal conductivity substantially decreases from monolayer to bilayer, but shows very little change for a further increase in the layer number. This layer dependence is similar to that observed at graphene [33] and is consistent with previous theoretical studies that predict a decrease in the thermal conductivity of 2D TMDC materials with an increase of the layer number [34].

We can gain more insight into the size and layer dependence of the thermal conductivity by comparing our result with that of bulk MoS_2. Previous studies have reported that the in-plane thermal conductivity of bulk MoS_2 varies between 85 and 110 W/m K, depending on the size of the incident laser beam. This dependence on the laser beam size corroborates the size dependence we observe at 2D MoS_2. Both an increase of the laser spot and the material size enable the involvement of thermal phonons with longer mean free paths. Additionally, the thermal conductivity of bulk MoS_2 is similar to that of large suspended monolayer MoS_2. This indicates that MoS_2 actually has similar thermal conductivity, regardless of the layer number, if the size is large enough. We believe that the observed layer dependence of the thermal conductivity is due to differences in the phonon properties [35] and the limited size of suspended MoS_2 flakes. The contribution of thermal phonons with a long mean free path (MFP) to thermal conduction could be larger in few-layer MoS_2 than that in monolayer MoS_2, and the micrometer-scale size of the few-layer flakes might only enable the involvement of part of the long MFP phonons. We expect that the thermal conductivity of few-layer MoS_2 will show thermal conductivity comparable to that of bulk MoS_2 if the size can be substantially increased.

The logarithmic size dependence of thermal conductivity holds for other 2D TMDC materials, such as WS_2 and WSe_2. Figure 3(c) shows the thermal conductivity measured from suspended single-crystalline monolayer WS_2 and WSe_2 flakes that are grown and transferred in ways

similar to the suspended MoS_2 flakes. The experimental conditions for the PSR and TC measurements of WS_2 and WSe_2 are also similar to those used for the measurement of monolayer MoS_2. Again, the thermal conductivity of monolayer WS_2 and WSe_2 increases with the suspended size, and the size dependence can be reasonably fitted with a logarithmic scaling as $k \sim \log(R)$. This is understandable because the logarithmic scaling is rooted in the two-dimensionality of the lattice, regardless of the specific composition [23–27]. For the TMDC materials measured, WS_2 has the highest thermal conductivity, followed by MoS_2 and WSe_2. The higher thermal conductivity of WS_2 than that of MoS_2 is surprising. Generally, phonon thermal conductivity is related to four parameters: atomic mass, interatomic bonding, crystal structures, and phonon anharmonicity [36]. All of these TMDC materials have similar crystal structures with negligible differences in phonon anharmonicity and atomic bonding. For instance, the difference in phonon anharmonicity (Gruneisen parameter) and atomic bonding between MoS_2 and WS_2 is around 6% and 4%, respectively [36]. However, the W atom is 40% heavier than the Mo atom, and WS_2 is intuitively expected to have a lower thermal conductivity than that of MoS_2, since heavier atoms tend to give rise to lower thermal conductivity. Our observed higher thermal conductivity of WS_2 is consistent with a recent theoretical study that also predicts a higher thermal conductivity in WS_2 than that in MoS_2 [28]. The theoretical study ascribes this to a larger phonon frequency gap between the acoustic and optical phonon branches in WS_2, which may result in less phonon-phonon scattering [28].

Apart from the in-plane thermal conductivity, we study the ITC of 2D TMDC materials and obtain further fundamental understanding as well. We use single-crystalline MoS_2 flakes with different layer numbers on sapphire substrates as an example to illustrate the main discovery. Similar to the suspended flakes, the layer number of the substrate-supported flakes can be identified from optical contrast and Raman measurements [Figs. 4(a) and 4(b)]. We perform Raman thermometry measurements on as-grown MoS_2 flakes on sapphire substrates [Figs. 4(c) and 4(d)]. The TC measurement conditions are similar to those used for the suspended flakes, but the PSR measurement of the supported flakes is conducted using a focused

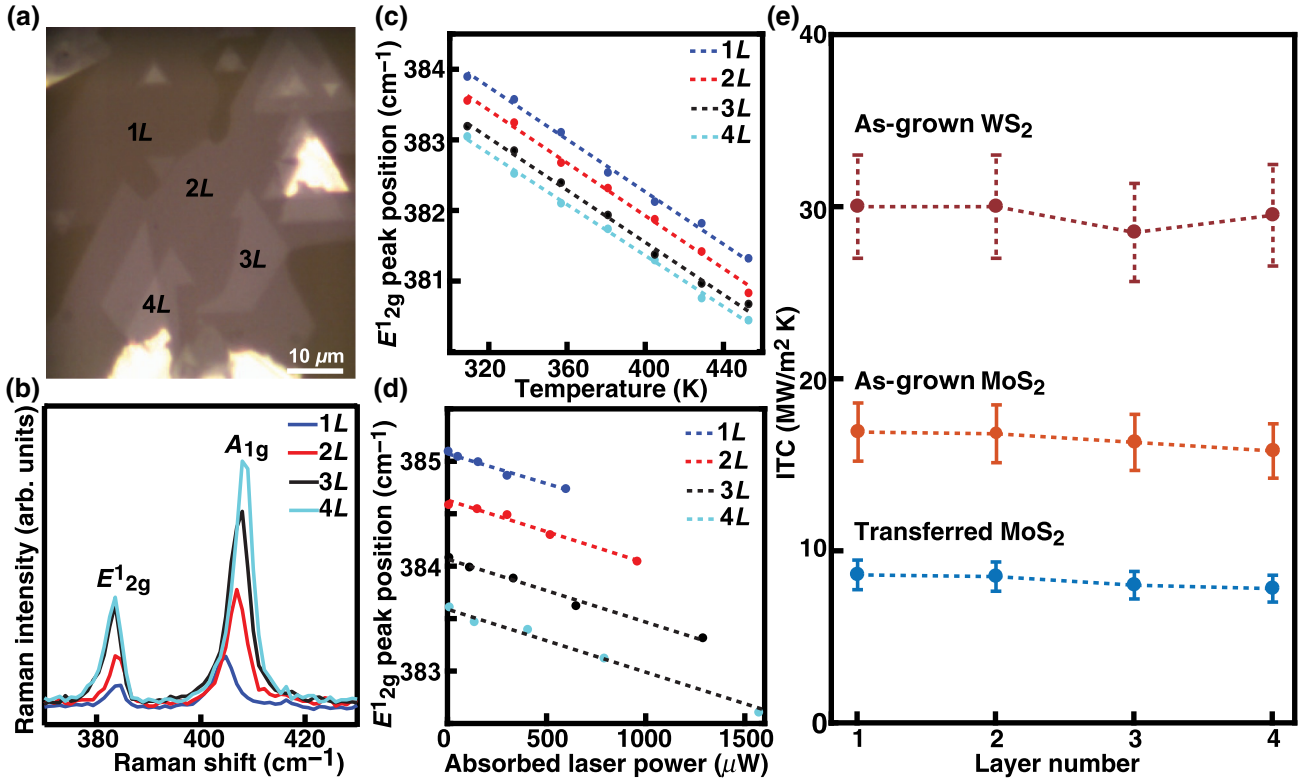

FIG. 4. Layer-independent interfacial thermal conductance of MoS_2. (a) Optical images of single-crystalline MoS_2 flakes with different layer numbers on sapphire substrates, in which layer numbers are labeled as shown. (b) Raman spectra of flakes with different layer numbers. Raman shift of E^1_{2g} peak of MoS_2 flakes as a function of (c) temperature and (d)absorbed laser power. Dots are experimental results and dashed lines are fits. TC measurement conditions are similar to those used for suspended flakes. PSR measurements are conducted using a focused 532 nm laser with a radius of 0.52 μm at room temperature. (e) Measured ITC of as-grown MoS_2 flakes (orange) and WS_2 flakes (red) on sapphire substrates as a function of layer number. Also plotted is the ITC of transferred MoS_2 flakes (blue) on sapphire substrates. Dots are experimental results and dashed lines serve as guides to the eye.

532 nm laser with a radius of 0.52 μm at room temperature. The ITC derived from fitting the measurement results with Eq. (9) is plotted in Fig. 4(e) (orange dots). Unlike the layer dependence of the in-plane thermal conductivity, the ITC of MoS_2 shows a negligible dependence on the layer number and is maintained at around 16–17 MW/m^2 K, regardless of the layer number [Fig. 4(e)]. Notably, we assume that all layers of few-layer MoS_2 are under thermal equilibrium (having the same temperature) in the derivation of the ITC from experimental measurements using Eqs. (6)–(9). This assumption is reasonable because the interlayer thermal conductance is much larger than the interfacial one between MoS_2 and underlying substrates. Previous studies have demonstrated that the interlayer thermal conductivity is 2.0 ± 0.3 W m^{-1} K^{-1} [37], and this corresponds to a interlayer thermal conductance of 6.33 GW m^{-2} K^{-1}, as the interlayer distance is 0.31 nm, which is more than two orders of magnitude larger than that of the interfacial thermal conductance. While we focus on MoS_2, the layer independence of the ITC holds true for other 2D materials. For instance, we measure the ITC of single-crystalline WS_2 flakes grown on sapphire substrates. The value is obviously larger ($\sim$30 MW/m^2 K) than that of the MoS_2 flakes, but it shows a similar layer independence of the layer number [Fig. 4(d) red dots]. Additionally, previous studies also reported the ITC of graphene to be independent of the layer number [38]. It is well accepted that the interfacial thermal conduction of dielectric materials is carried out by the interfacial transfer of phonons and governed by two factors, matching of the phonon spectra of the objects involved and strength of the interfacial bonding [39–41]. The observed layer independence of the ITC implies no layer dependence in the phonon spectra matching and interaction between substrates and MoS_2.

Our experimental result indicates that the ITC of 2D TMDC materials strongly depends on the strength of the interaction between the materials and the substrates. We measure the ITC of MoS_2 flakes transferred from growth substrates (sapphire) onto another sapphire substrate. Transfer follows a surface-energy-assisted transfer process we developed previously, and we confirm no degradation in the quality of the flakes during the transfer process [14]. The ITC of the transferred flakes shows no dependence on the layer number either (blue dots in Fig. 4(e)), but is 40%–50% lower than that of the as-grown counterparts, in the range of 8–10 MW/m^2 K. This is because the transferred flakes interact with the substrates less intimately than the as-grown counterparts. We also measure the ITC of monolayer MoS_2 flakes transferred onto other substrates. The ITC substantially varies with the substrates, for instance, GaN (6.1 ± 1.0 MW/m^2 K), Au (8.0 ± 1.2 MW/m^2 K), Cu (7.1 ± 1.1 MW/m^2 K), Ni (2.3 ± 0.5 MW/m^2 K), and HOPG (13 ± 2.0 MW/m^2 K). A detailed discussion of the mechanism underlying the substrate-dependent variation is beyond the scope of this work. However, we believe that the interaction strength of MoS_2 with the substrates plays an important role in the observed substrate-dependent variation. For instance, 2D material substrates, such as HOPG, may enable a higher ITC than that of conventional 3D substrates because 2D TMDC materials interact with the 2D substrate more strongly than that with 3D substrates. Au and Cu may enable a higher ITC than those of many other metals because Au and Cu have a tendency to form covalent bonds with sulfur atoms, even under ambient conditions [42].

From the standpoint of device development, it is important to understand the ITC of 2D TMDC materials on silicon substrates with thermally grown silicon oxides, which are expected to be widely used in 2D TMDC material devices. We perform Raman thermometry measurements at as-grown MoS_2 flakes on SiO_2/Si substrates with different thicknesses of the SiO_2 layer and use the abovementioned analytical model to extract the ITC. The result is plotted in Fig. 5(a). The ITC shows no dependence on the layer number [Fig. 5(a), inset], but monotonically decreases with an increase in the thickness of the SiO_2 layer [Fig. 5(a)]. The result shown in Fig. 5(a) actually represents the effective interfacial thermal conduction collectively contributed to by multiple steps in the system. As illustrated in Fig. 5(b), inset, these steps include interfacial thermal conduction between 2D MoS_2 and SiO_2 (G_{2D/SiO_2}), thermal conduction in the SiO_2 layer (k_{SiO_2}), interfacial thermal conduction at the SiO_2/Si interface ($G_{SiO_2/Si}$), and thermal conduction in Si (k_{Si}). We expect $G_{SiO_2/Si}$ (>600 MW/m^2 K) [43] and k_{Si} (130 W/m K) [44] to be much larger than that of G_{2D/SiO_2} and k_{SiO_2}, and this is supported by the negligible temperature increase at the Si substrate during Raman thermometry measurements (Fig. S3 within the Supplemental Material [20]). Therefore, the effective thermal conductance G_{eff} may be correlated to G_{2D/SiO_2} and k_{SiO_2} as $1/G_{eff} = 1/G_{2D/SiO_2} + d/k_{SiO_2}$, where d is the thickness of the SiO_2 layer. The true interfacial thermal conductance, G_{2D/SiO_2}, can be determined from the measured effective ITC G_{eff}. We plot the reciprocal of the result in Fig. 5(a) ($1/G_{eff}$) as a function of the thickness of the SiO_2 layer in Fig. 5(b). A linear fitting of the result indicates that G_{2D/SiO_2} is 18.6 MW/m^2 K, and the thermal conductivity of thermally grown SiO_2 k_{SiO_2} is around 1.377 W/m K [45], both of which are reasonably consistent with results reported in Refs. [46–48].

Our result clarifies much inconsistency in the thermal conduction properties of 2D materials reported in the literature. For instance, the in-plane thermal conductivity of 2D MoS_2 reported in the literature shows substantial variation [10,37,49–53]. We find that one major reason for the variation lies in the difference in sample size and layer number. To illustrate this idea, we summarize the previously reported thermal conductivities of MoS_2 along with our results in Table I. The previous results include the thermal

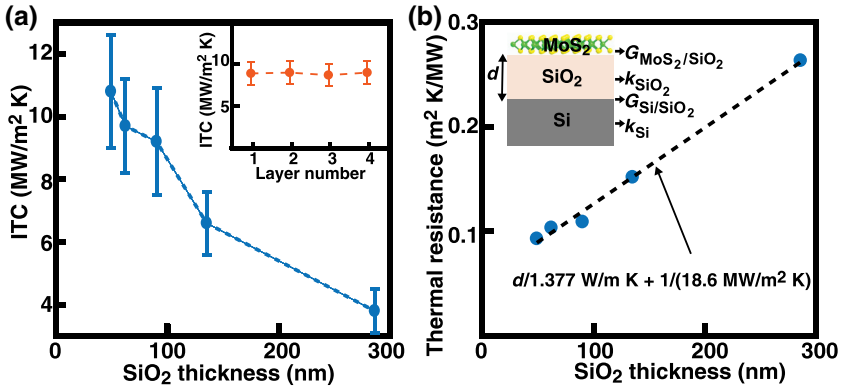

FIG. 5. Interfacial thermal conductance of monolayer MoS_2 on SiO_2/Si substrates with different SiO_2 thicknesses. (a) Measured effective ITC of MoS_2 on SiO_2/Si substrates as a function of thickness of the SiO_2 layer. Inset: measured ITC of MoS_2 flakes with different layer numbers on SiO_2/Si substrates. TC measurement conditions are similar to those used for suspended flakes. PSR measurements are conducted using a focused 532 nm laser with a radius of 0.52 μm at room temperature. (b) Reciprocal of effective ITC (thermal resistance) as a function of thickness of the SiO_2 layer, in which the error bar is removed for clarity. Dashed line is a linear fitting. Inset schematically illustrates all steps involved in thermal dissipation of MoS_2 on SiO_2/Si substrates with 90 nm thermally grown SiO_2.

conductivities measured using either Raman thermometry or microbridge and at materials prepared by either CVD processes or exfoliation. To ensure a fair comparison, we list only the results in the references that provide enough experimental details (such absorption efficiency, suspended size, and layer number) to allow us to reanalyze the measurement results. As shown in Table I, regardless of the measurement techniques and preparation method, most of the previous results are reasonably consistent with our results. The consistence of our results with the results obtained from microbridge measurements also supports the accuracy of our Raman thermometry measurements.

TABLE I. Comparison of thermal conductivities measured at suspended MoS_2.

Ref.	Method	Layer number	Suspended size (μm)	Thermal conductivity (W/m K)	Sample type
This work	Raman	**1**	Radius: 1.8	32.5 ± 3.4	CVD
Yan *et al.* [10]	Raman	1	Radius: 0.6	34.5 ± 4	Exfoliated
Bae *et al.* [9]	Raman	1	Radius: 1.8	36.6 (13.3 ± 1.4)[a]	CVD
Yarali *et al.* [11]	Microbridge	1	Length: 1.31 ± 0.06 Width: 8.38 ± 0.89	30 ± 3.3	CVD
Yarali *et al.* [11]	Microbridge	1	Length: 1.1 ± 0.063 Width: 10.8 ± 0.63	35.5 ± 3	CVD
Zhang *et al.* [12][b]	Raman	1	Radius: 2.0	84 ± 17	Exfoliated
This work	Raman	2	Radius: 1.8	18.1 ± 1.8	CVD
Zhang *et al.* [12][b]	Raman	2	Radius: 2.0	77 ± 25	Exfoliated
Bae *et al.* [9]	Raman	2	Radius: 1.8	15.6 ± 1.5	CVD
This work	Raman	4	Radius: 4.0	36.9 ± 4.9	CVD
Jo *et al.* [51]	Microbridge	4	Length: 3.0 Width: 5.2	44–50	Exfoliated
Aiyiti *et al.* [49]	Microbridge	4	Length: 2.0 Width: 3.0	34 ± 5	Exfoliated
Aiyiti *et al.* [49]	Microbridge	4	Length: 3.0 Width: 3.82	31 ± 4	Exfoliated
Aiyiti *et al.* [49]	Microbridge	5	Length: 1.0 Width: 5.87	30 ± 3	Exfoliated
Jo *et al.* [51]	Microbridge	7	Length: 8.0 Width: 2.2	48-52	Exfoliated
Bae *et al.* [9]	Raman	(10–14)	Radius: 1.8	43.4 ± 9.1	CVD

[a]The value in parentheses is the original value presented in the paper, and 36.6 is what we obtain using the correct absorption efficiency.
[b]These results are somehow different from ours.

Additionally, many previous studies reported the ITC of 2D materials on SiO_2/Si substrates [12,22,38,47], but little attention has been paid to the effect of the thickness of the SiO_2 layer on the measurement results.

Our results also provide useful guidance for the thermal management of 2D TMDC materials. They suggest that the interfacial thermal conduction would be dominant over the in-plane thermal conduction for the heat dissipation of 2D TMDC materials. We use substrate-supported 2D material devices with a circular heating zone with a radius of r as an example to illustrate this idea. The power dissipation by the interfacial (P_I) and lateral (P_L) thermal conduction may be written as $P_I = g\pi r^2 \Delta T$ and $P_L = 2\pi rtkdT/dr$, respectively. For simplicity, we assume that the temperature gradient in the lateral direction is linear and confined to the heating zone, i.e., $dT/dr = \Delta T/r$. Then P_L can be written as $P_L = 2\pi kt\Delta T$. For the interfacial thermal conduction to be more efficient in heat dissipation, we need to have $gr^2 \geq 2kt$, which gives rise to $r \geq (2kt/g)^{1/2}$. While we measure the in-plane thermal conductivity at suspended 2D TMDC materials, the thermal conductivity of substrate-supported 2D TMDC materials is expected to be similar to that of suspended few layers. This is because the substrate effects could be similar to the effect of adding more layers [38,54–56]. Without losing generality, we consider $k = 20$ W/m K and $g = 2$–20 MW/m^2 K, and the critical value of $(2kt/g)^{1/2}$ is in the range of 30–100 nm. Any practical device would have a heating area larger than this (even a single field-effect transistor in integrated circuits could be of smaller size, but the overall size of a practical integrated circuit would be much larger). Therefore, engineering the interfacial thermal conduction should be the main strategy for the thermal management of 2D TMDC materials and devices. Our results also indicate that using different numbers of layers does not make any substantial difference to the interfacial thermal conduction, but engineering the substrates, such as the interaction strength with the materials and the thickness of the oxide layer in Si/SiO_2 substrates, provides an efficient strategy to control the heat dissipation of 2D TMDC materials.

IV. CONCLUSION

We present a fundamental understanding of the thermal conduction of 2D TMDC materials, including in-plane thermal conductivity and interfacial thermal conductance. We elucidate the dependence of thermal conduction on the physical features of the system, including size, layer number, composition, and substrates. Most importantly, we find that the in-plane thermal conductivity k increases with the radius R of the suspended area, following a logarithmic scaling, as $k \sim \log(R)$. k also shows some dependence on the layer number, substantially decreasing from monolayer to bilayer, but only changing slightly with a further increase in the layer number. In contrast, the interfacial thermal conductance g shows little dependence on the layer number, but g increases with the strength of the interaction between 2D TMDC materials and the substrate, substantially varying among different substrates. Our results are consistent with the prediction of many theoretical studies and clarify many inconsistencies in the results from previous studies.

ACKNOWLEDGMENTS

This work is supported by a CAREER award from the National Science Foundation (DMR-1352028) and partially by grants ECCS-1508856 and EFMA 1741693 from the National Science Foundation. The authors acknowledge Dr. Y. Zhu for providing access to a Horiba Labram HR800 system and Chen Zhang for assistance with the synthesis of WSe_2 flakes, and acknowledge use of the Analytical Instrumentation Facility (AIF) at North Carolina State University, which is supported by the State of North Carolina and the National Science Foundation.

[1] A. Allain and A. Kis, Electron and hole mobilities in single-layer WSe_2, ACS Nano **8**, 7180 (2014).
[2] M. Bernardi, C. Ataca, M. Palummo, and J. C. Grossman, Optical and electronic properties of two-dimensional layered materials, Nanophotonics **6**, 479 (2017).
[3] H. Wang, L. Yu, Y.-H. Lee, Y. Shi, A. Hsu, M. L. Chin, L.-J. Li, M. Dubey, J. Kong, and T. Palacios, Integrated circuits based on bilayer MoS_2 transistors, Nano Lett. **12**, 4674 (2012).
[4] S. Salehi and A. Saffarzadeh, Optoelectronic properties of defective MoS_2 and WS_2 monolayers, J. Phys. Chem. Solids **121**, 172 (2018).
[5] N. Zibouche, A. Kuc, J. Musfeldt, and T. Heine, Transition-metal dichalcogenides for spintronic applications, Ann. Phys-Berlin **526**, 395 (2014).
[6] W. Wu, L. Wang, Y. Li, F. Zhang, L. Lin, S. Niu, D. Chenet, X. Zhang, Y. Hao, and T. F. Heinz, Piezoelectricity of single-atomic-layer MoS_2 for energy conversion and piezotronics, Nature **514**, 470 (2014).
[7] K. Hippalgaonkar, Y. Wang, Y. Ye, D. Y. Qiu, H. Zhu, Y. Wang, J. Moore, S. G. Louie, and X. Zhang, High thermoelectric power factor in two-dimensional crystals of MoS_2, Phys. Rev. B **95**, 115407 (2017).
[8] X. Gu and R. Yang, Phonon transport and thermal conductivity in two-dimensional materials, Annu. Rev. Heat Transfer **19**, 1 (2016).
[9] J. J. Bae, H. Y. Jeong, G. H. Han, J. Kim, H. Kim, M. S. Kim, B. H. Moon, S. C. Lim, and Y. H. Lee, Thickness-dependent in-plane thermal conductivity of suspended MoS_2 grown by chemical vapor deposition, Nanoscale **9**, 2541 (2017).
[10] R. Yan, J. R. Simpson, S. Bertolazzi, J. Brivio, M. Watson, X. Wu, A. Kis, T. Luo, A. R. Hight Walker, and H. G. Xing, Thermal conductivity of monolayer molybdenum disulfide obtained from temperature-dependent Raman spectroscopy, ACS Nano **8**, 986 (2014).

[11] M. Yarali, X. Wu, T. Gupta, D. Ghoshal, L. Xie, Z. Zhu, H. Brahmi, J. Bao, S. Chen, and T. Luo, Effects of defects on the temperature-dependent thermal conductivity of suspended monolayer molybdenum disulfide grown by chemical vapor deposition, Adv. Func. Mater. **27**, 1704357 (2017).

[12] X. Zhang, D. Sun, Y. Li, G.-H. Lee, X. Cui, D. Chenet, Y. You, T. F. Heinz, and J. C. Hone, Measurement of lateral and interfacial thermal conductivity of single-and bilayer MoS_2 and $MoSe_2$ using refined optothermal Raman technique, ACS Appl. Mater. Interfaces **7**, 25923 (2015).

[13] Y. H. Lee, X. Q. Zhang, W. Zhang, M. T. Chang, C. T. Lin, K. D. Chang, Y. C. Yu, J. T. W. Wang, C. S. Chang, and L. J. Li, Synthesis of large-area MoS_2 atomic layers with chemical vapor deposition, Adv. Mater **24**, 2320 (2012).

[14] A. Gurarslan, Y. Yu, L. Su, Y. Yu, F. Suarez, S. Yao, Y. Zhu, M. Ozturk, Y. Zhang, and L. Cao, Surface-energy-assisted perfect transfer of centimeter-scale monolayer and few-layer MoS_2 films onto arbitrary substrates, ACS Nano **8**, 11522 (2014).

[15] W. W. Cai, A. L. Moore, Y. W. Zhu, X. S. Li, S. S. Chen, L. Shi, and R. S. Ruoff, Thermal transport in suspended and supported monolayer graphene grown by chemical vapor deposition, Nano Lett. **10**, 1645 (2010).

[16] J. Judek, A. P. Gertych, M. Swiniarski, A. Lapinska, A. Duzynska, and M. Zdrojek, High accuracy determination of the thermal properties of supported 2D materials, Sci. Rep **5**, 1 (2015).

[17] H. Malekpour and A. A. Balandin, Raman-based technique for measuring thermal conductivity of graphene and related materials, J. Raman Spectrosc **49**, 106 (2018).

[18] Y. Yu, Y. Yu, Y. Cai, W. Li, A. Gurarslan, H. Peelaers, D. E. Aspnes, C. G. V. d. Walle, N. V. Nguyen, Y.-W. Zhang, and L. Cao, Exciton-dominated dielectric function of atomically thin MoS_2 films, Sci. Rep. **5**, 16996 (2015).

[19] Y. Yu, Y. Yu, L. Huang, H. Peng, L. Xiong, and L. Cao, Giant gating tunability of optical refractive index in transition metal dichalcogenide monolayers, Nano Lett. **17**, 3613 (2017).

[20] See the Supplemental Material at http://link.aps.org/supplemental/10.1103/PhysRevApplied.13.034059 for more data on the Raman photothermometry measurements and tabulated experimental data.

[21] Y. Li, A. Chernikov, X. Zhang, A. Rigosi, H. M. Hill, A. M. van der Zande, D. A. Chenet, E.-M. Shih, J. Hone, and T. F. Heinz, Measurement of the optical dielectric function of monolayer transition-metal dichalcogenides: MoS_2, Mo Se_2, WS_2, and WS e_2, Phys. Rev. B **90**, 205422 (2014).

[22] E. Yalon, O. Z. R. B. Aslan, K. K. Smithe, C. J. McClellan, S. V. Suryavanshi, F. Xiong, A. Sood, C. M. Neumann, X. Xu, and K. E. Goodson, Temperature-dependent thermal boundary conductance of monolayer MoS_2 by Raman thermometry, ACS Appl. Mater. Interfaces **9**, 43013 (2017).

[23] S. Lepri, R. Livi, and A. Politi, Studies of thermal conductivity in Fermi–pasta–ulam-like lattices, chaos: An interdisciplinary, J. Nonlinear Sci. **15**, 015118 (2005).

[24] L. Wang, B. Hu, and B. Li, Logarithmic divergent thermal conductivity in two-dimensional nonlinear lattices, Phys. Rev. E **86**, 040101 (2012).

[25] L. Wang, N. Li, and P. Hänggi, *Thermal Transport in Low Dimensions* (Springer, New York, 2016), p. 239.

[26] D. Xiong, J. Wang, Y. Zhang, and H. Zhao, Heat conduction in two-dimensional disk models, Phys. Rev. E **82**, 030101 (2010).

[27] L. Yang, P. Grassberger, and B. Hu, Dimensional crossover of heat conduction in low dimensions, Phys. Rev. E **74**, 062101 (2006).

[28] X. Gu and R. Yang, Phonon transport in single-layer transition metal dichalcogenides: A first-principles study, Appl. Phys. Lett. **105**, 131903 (2014).

[29] K. Xu, A. J. Gabourie, A. Hashemi, Z. Fan, N. Wei, A. B. Farimani, H.-P. Komsa, A. V. Krasheninnikov, E. Pop, and T. Ala-Nissila, Thermal transport in MoS_2 from molecular dynamics using different empirical potentials, Phys. Rev. B **99**, 054303 (2019).

[30] M.-H. Bae, Z. Li, Z. Aksamija, P. N. Martin, F. Xiong, Z.-Y. Ong, I. Knezevic, and E. Pop, Ballistic to diffusive crossover of heat flow in graphene ribbons, Nat. Commun. **4**, 1734 (2013).

[31] X. Xu, L. F. Pereira, Y. Wang, J. Wu, K. Zhang, X. Zhao, S. Bae, C. T. Bui, R. Xie, and J. T. Thong, Length-dependent thermal conductivity in suspended single-layer graphene, Nat. Commun. **5**, 3689 (2014).

[32] Y. Cai, J. Lan, G. Zhang, and Y.-W. Zhang, Lattice vibrational modes and phonon thermal conductivity of monolayer MoS_2, Phys. Rev. B **89**, 035438 (2014).

[33] H.-Y. Cao, Z.-X. Guo, H. Xiang, and X.-G. Gong, Layer and size dependence of thermal conductivity in multilayer graphene nanoribbons, Phys. Lett. A **376**, 525 (2012).

[34] Y. F. Yu, Y. L. Yu, C. Xu, Y. Q. Cai, L. Q. Su, Y. Zhang, Y. W. Zhang, K. Gundogdu, and L. Y. Cao, Engineering substrate interactions for high luminescence efficiency of transition-metal dichalcogenide monolayers, Adv. Func. Mater **26**, 4733 (2016).

[35] L. Lindsay and D. Broido, Theory of thermal transport in multilayer hexagonal boron nitride and nanotubes, Phys. Rev. B **85**, 035436 (2012).

[36] B. Peng, H. Zhang, H. Shao, Y. Xu, X. Zhang, and H. Zhu, Thermal conductivity of monolayer MoS_2, $MoSe_2$, and WS_2: Interplay of mass effect, interatomic bonding and anharmonicity, RSC Adv. **6**, 5767 (2016).

[37] J. Liu, G.-M. Choi, and D. G. Cahill, Measurement of the anisotropic thermal conductivity of molybdenum disulfide by the time-resolved magneto-optic Kerr effect, J. Appl. Phys. **116**, 233107 (2014).

[38] K. F. Mak, C. H. Lui, and T. F. Heinz, Measurement of the thermal conductance of the graphene/SiO_2 interface, Appl. Phys. Lett. **97**, 221904 (2010).

[39] R. Prasher, Acoustic mismatch model for thermal contact resistance of van der Waals contacts, Appl. Phys. Lett. **94**, 041905 (2009).

[40] E. T. Swartz and R. O. Pohl, Thermal-boundary resistance, Rev. Mod. Phys. **61**, 605 (1989).

[41] H. B. Zhou and G. Zhang, General theories and features of interfacial thermal transport, Chin. Phys. B **27**, 034401 (2018).

[42] X. Liu, G. Zhang, and Y.-W. Zhang, Thermal conduction across the one-dimensional interface between a MoS_2 monolayer and metal electrode, Nano Res. **9**, 2372 (2016).

[43] J. Kimling, A. Philippi-Kobs, J. Jacobsohn, H. P. Oepen, and D. G. Cahill, Thermal conductance of interfaces with

amorphous SiO_2 measured by time-resolved magneto-optic kerr-effect thermometry, Phys. Rev. B **95**, 184305 (2017).

[44] C. J. Glassbrenner and G. A. Slack, Thermal conductivity of silicon+germanium from 3 degrees K to melting point, Phys. Rev. **134**, 1058 (1964).

[45] A. S. Grove, *Physics and Technology of Semiconductor Devices* (Wiley, New York, 1967).

[46] E. Yalon, O. B. Aslan, K. K. H. Smithe, C. J. McClellan, S. V. Suryavanshi, F. Xiong, A. Sood, C. M. Neumann, X. Q. Xu, K. E. Goodson, T. F. Heinz, and E. Pop, Temperature-Dependent thermal boundary conductance of monolayer MoS_2 by Raman thermometry, ACS Appl. Mater. Interfaces **9**, 43013 (2017).

[47] E. Yalon, C. J. McClellan, K. K. H. Smithe, M. M. Rojo, R. L. Xu, S. V. Suryavanshi, A. J. Gabourie, C. M. Neumann, F. Xiong, A. B. Farimani, and E. Pop, Energy dissipation in monolayer MoS_2 electronics, Nano Lett. **17**, 3429 (2017).

[48] P. Yasaei, C. J. Foss, K. Karis, A. Behranginia, A. I. El-Ghandour, A. Fathizadeh, J. Olivares, A. K. Majee, C. D. Foster, F. Khalili-Araghi, Z. Aksamija, and A. Salehi-Khojin, Interfacial thermal transport in monolayer MoS_2- and graphene-based devices, Adv. Mater. Interfaces **4**, 1700334 (2017).

[49] A. Aiyiti, X. Bai, J. Wu, X. Xu, and B. Li, Measuring the thermal conductivity and interfacial thermal resistance of suspended MoS_2 using electron beam self-heating technique, Sci. Bull. **63**, 452 (2018).

[50] X. Gu, Y. Wei, X. Yin, B. Li, and R. Yang, Colloquium: Phononic thermal properties of two-dimensional materials, Rev. Mod. Phys. **90**, 041002 (2018).

[51] I. Jo, M. T. Pettes, E. Ou, W. Wu, and L. Shi, Basal-plane thermal conductivity of few-layer molybdenum disulfide, Appl. Phys. Lett. **104**, 201902 (2014).

[52] N. Peimyoo, J. Shang, W. Yang, Y. Wang, C. Cong, and T. Yu, Thermal conductivity determination of suspended mono-and bilayer WS_2 by Raman spectroscopy, Nano Res. **8**, 1210 (2015).

[53] S. Sahoo, A. P. Gaur, M. Ahmadi, M. J.-F. Guinel, and R. S. Katiyar, Temperature-dependent Raman studies and thermal conductivity of few-layer MoS_2, The J. Phys. Chem. C **117**, 9042 (2013).

[54] Y. Hong, L. Li, X. C. Zeng, and J. Zhang, Tuning thermal contact conductance at graphene–copper interface via surface nanoengineering, Nanoscale **7**, 6286 (2015).

[55] Y. K. Koh, M.-H. Bae, D. G. Cahill, and E. Pop, Heat conduction across monolayer and few-layer graphenes, Nano Lett. **10**, 4363 (2010).

[56] Z. Chen, W. Jang, W. Bao, C. Lau, and C. Dames, Thermal contact resistance between graphene and silicon dioxide, Appl. Phys. Lett. **95**, 161910 (2009).